NANO LETTERS

pubs.acs.org/NanoLett Letter

Overcoming Li^+ Transport Hysteresis via Bio-Inspired Neuron-Like 3D Carbon Framework Engineering for Stable Li Metal Anode

Bo Zhang,[▽] Donghu Li,[▽] Xinli Wu, Jitao Huang, Shi Wang,* Lifeng Hou, Yinghui Wei,* Qian Wang,* and Zhong Jin*

Cite This: *Nano Lett.* 2026, 26, 3330−3337 Read Online

ACCESS | Metrics & More | Article Recommendations | Supporting Information

ABSTRACT: Li metal is a promising anode for next-generation batteries owing to its ultrahigh specific capacity and low redox potential, yet practical use is hampered by dendrite formation and large volume fluctuations. Composite Li anodes can spatially confine active Li, but their cycling durability remains limited by uncontrolled interfacial Li^+ transport. Inspired by the rapid signal conduction of biological neurons, we develop a lithiophilic, neuron-like 3D carbon framework derived from an N-rich melamine polymer as an advanced Li host. This architecture provides continuous, low-hysteresis Li^+ transport pathways, while abundant N dopants create uniformly distributed nucleation sites and mitigate plating/stripping-induced strain. As a result, the composite anode achieves 98.6% Coulombic efficiency over 800 cycles in half cells and stable cycling for 2000 h in symmetric cells, with full cells showing excellent retention at low N/P ratios. This work offers a cost-effective strategy for regulating interfacial Li^+ transport in Li anodes.

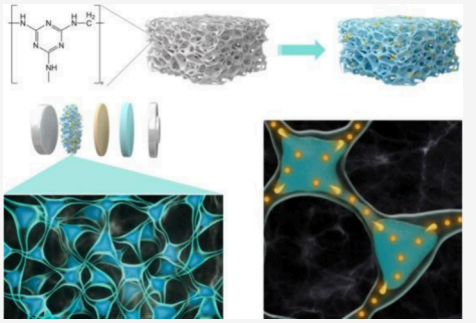

KEYWORDS: *Li metal batteries, Composite Li metal anode, Neuron-like 3D framework, N-rich host, SEI*

Continuously improving the energy density of Li ion batteries is the key to alleviating range anxiety in electric vehicles, and Li metal has been widely regarded as a leading anode candidate for the next-generation rechargeable batteries with high energy density, owing to its high theoretical specific capacity (3860 mAh g^{-1}) and the lowest electrochemical potential (−3.04 V vs SHE).[1] However, the practical application of Li metal anode remains severely limited by the uncontrolled Li dendrite growth and huge volume fluctuations during charge/discharge process.[2,3]

To address these issues, researchers have developed various strategies over the past decades, such as surface modification,[3] electrolyte regulation,[4] constructing three-dimensional composite Li metal anode,[5] etc. Among them, a composite Li anode can disperse and bind Li metal in 3D space, improving safety while suppressing the volume effect and dendrite growth. Up to now, numerous frameworks have been developed, mainly including: carbon fiber frameworks,[6] graphene frameworks,[7] 3D metal skeletons,[8] porous carbon with vertical nanochannels,[9] etc. However, current research generally overlooks the multidimensional complex interface problems caused by 3D composite systems, especially the new local interfaces formed between the internal microstructure of the framework and the electrolyte. The Li^+ migration and transformation behavior in 3D composite systems exhibit significant spatial heterogeneity. To this end, researchers have further functionalized conventional 3D framework materials to regulate the Li nucleation and growth process at local interfaces, such as modifying lithiophilic metal nanoparticles (Ag, Au, etc.),[10−12] regulating surface electronic structure and constructing multicomponent,[13] cross scale 3D framework materials.[14]

Nevertheless, there is still an undeniable issue with these strategies, namely controllability. For example, there is still uneven distribution of lithiophilic metal nanoparticles during the modification process, which will lead to uneven Li^+ migration and conversion behavior at the local interface. Recently, the skeleton material with a neuron-like structure has attracted significant attention. Inspired by the rapid transmission of electrical/chemical signals by biological neurons, this structure can synergistically regulate the transport of electrons and Li^+ ions inside the electrode. For example, the Zhang group proposed a biomimetic fiber electrode design with the neuron-like structure, which consists of a one-dimensional conductive skeleton (axon-like) and a two-dimensional active unit (cell-like).[15] This structure overcomes the challenge of electron−ion transport hysteresis at the fiber electrode interface and effectively enhances Li^+ transport kinetics. However, the functionalized neuron-like structure still exhibits poor lithiophilicity and when directly applied to

Received: October 10, 2025
Revised: January 7, 2026
Accepted: January 8, 2026
Published: March 9, 2026

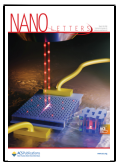

https://doi.org/10.1021/acs.nanolett.5c05102
Nano Lett. 2026, 26, 3330−3337

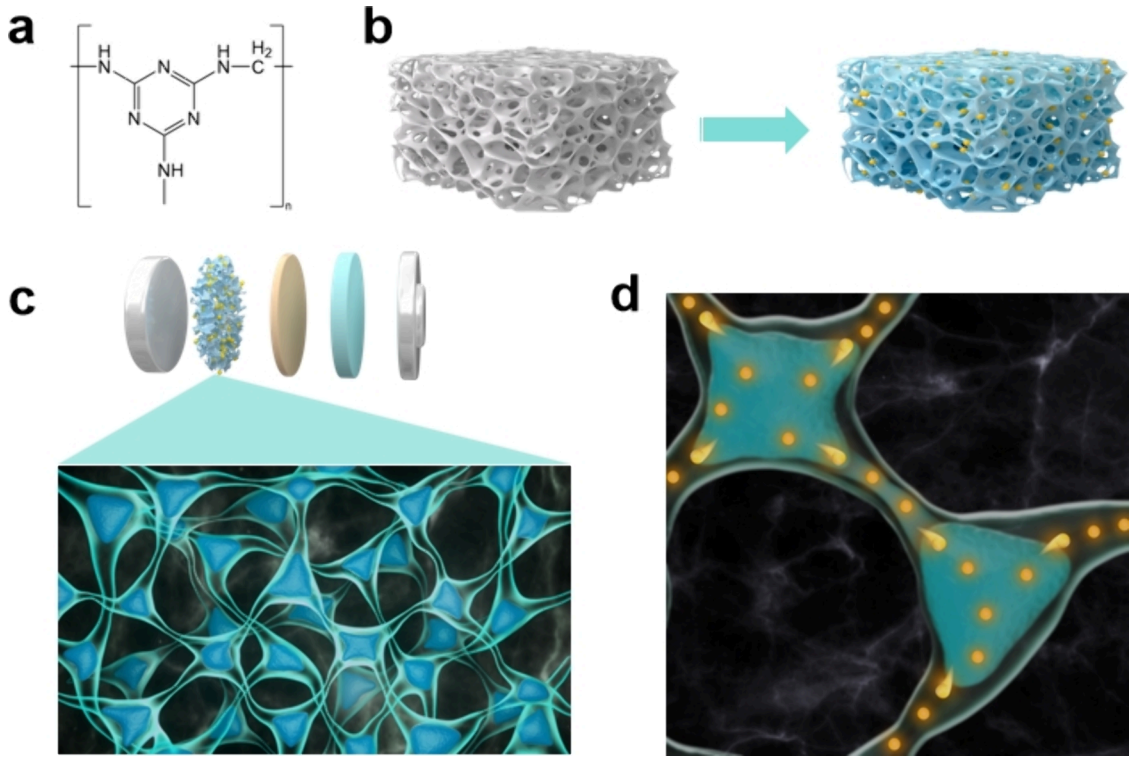

Figure 1. Design concept and skeleton feature. (a) The structure formula of melamine foam (MF). (b) Schematic diagram of the carbonization process of MF skeleton, where the yellow ball is the N element. (c, d) Schematic diagram of neuron-like 3D carbon framework and Li^+ flux.

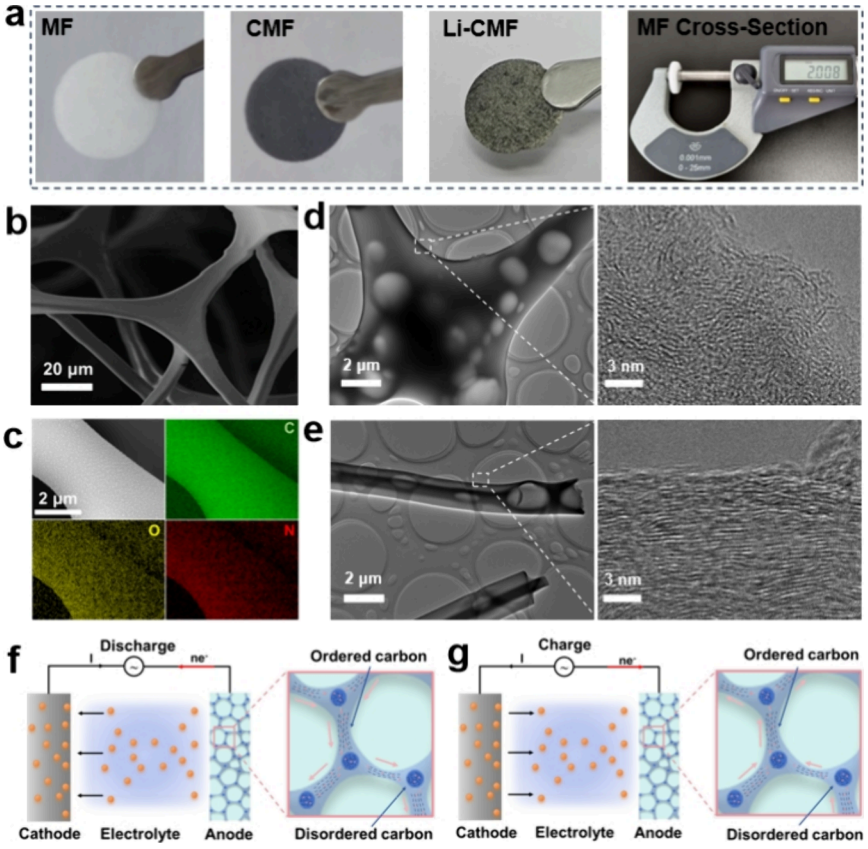

Figure 2. Nucleation and deposition behavior. (a) Optical photographs of MF, CMF, Li-CMF, and MF cross-section. (b) SEM image and high-resolution transmission electron microscopy (HRTEM) images of CMF and amorphous carbon at the nodules (c). (d) Elemental mapping images of CMF. (e) HRTEM images of ordered carbon structure at the branches. (f, g) Schematic diagram of electron transfer during charging and discharging.

https://doi.org/10.1021/acs.nanolett.5c05102
Nano Lett. 2026, 26, 3330−3337

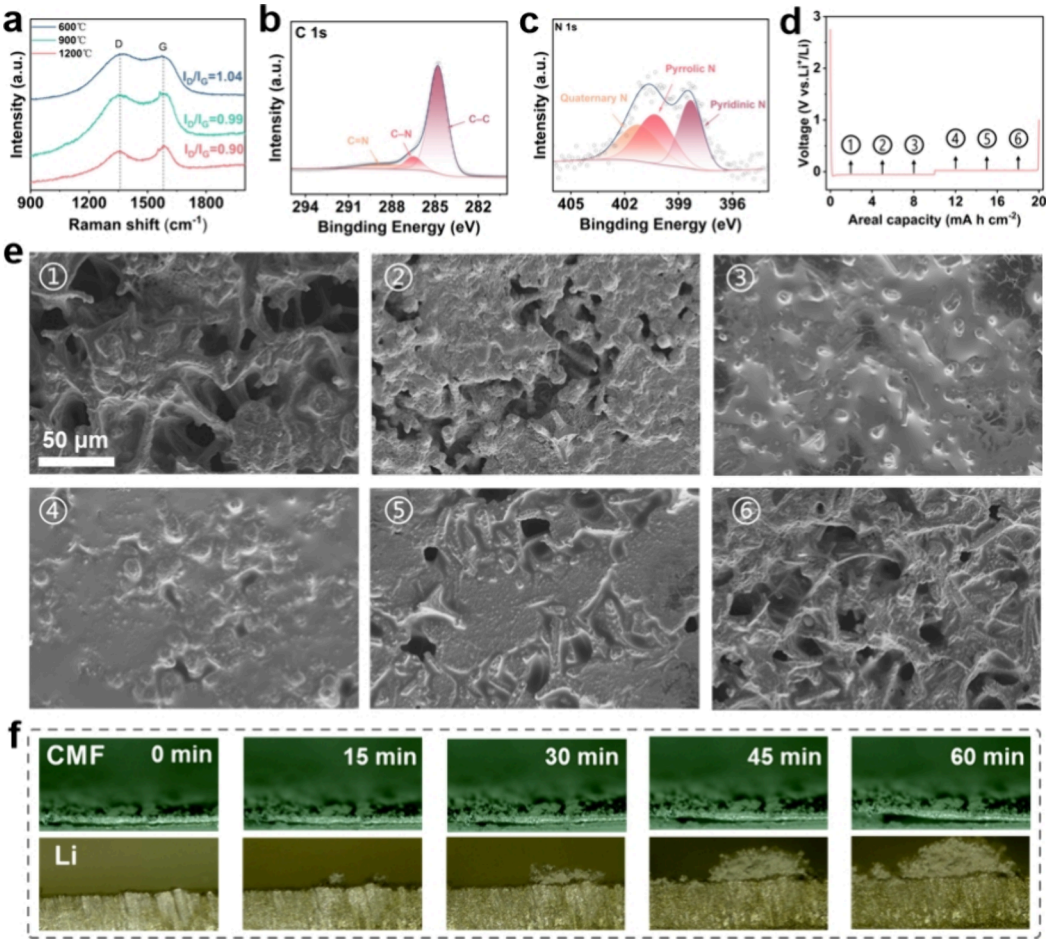

Figure 3. Electrochemical stability. (a) Raman spectra of CMF at different carbonization temperatures. (b, c) XPS spectrum of C 1s (b) and N 1s (c). (d) Li plating/stripping voltage curves of CMF at 1.0 mA cm^{-2} with the capacity of 10 mAh cm^{-2}. (e) Ex situ SEM images of CMF at different deposition/stripping stages in (d). (f) In situ optical microscopy duing Li deposition process.

composite Li metal anode, Li dendrite still forms, holding significant promise for realizing its practical application.

Herein, this work constructed a highly lithiophilic and neuron-like 3D framework by carbonizing a N-rich melamine polymer (Figure 1a and b). Specifically, this framework exhibited distinct arrangements of C atoms at the nodal junctions and along the fiber segments, forming a heterogeneous network analogous to biological neuronal structure. This unique structural configuration facilitated continuous and low-hysteresis Li^+ transport pathways, while its abundant active N sites can efficiently capture Li^+ during the Li plating/stripping process, alleviating the interfacial kinetic limitations (Figure 1c).

Benefiting from the significantly controlled Li^+ transport pathways and effective Li^+ transport kinetics enabled by this neuron-like carbon framework, the composite Li metal anode demonstrated a high CE of 98.6% over 800 cycles at a current density of 1.0 mA cm^{-2}. And even at a low N/P ratio, the full cells with $LiFePO_4$ (LFP) cathode displayed a high capacity retention of >95% after 500 cycles at 1.0 C. This work offers an effective and scalable strategy for high-performance Li metal anodes.

For the bare Li metal anode, its severe volume expansion during charging and discharging can damage the SEI layer on the electrode surface, leading to the formation of Li dendrites after long cycles. Therefore, Li metal is usually coupled with a 3D framework to construct a composite Li metal anode in order to minimize the volume change during cycling. However, the current framework still faces significant challenges in regulating the Li^+ nucleation and migration behavior. Thus, we constructed a functional skeleton with neuron-like structure for a composite Li metal anode. As shown in Figure 2a, we choose the common melamine foam (MF) as the precursor and obtained a conductive functional skeleton through high-temperature carbonization, named as CMF. During the carbonization process, size shrinkage occurred due to thermal condensation, and the CMF retained its original porous structure while forming a functionalized skeleton with a neuron-like structure. As shown in Figure 2b and Figure S1, the average diameter of the fibers on the functionalized skeleton was about 6.2 μm. Furthermore, we optimized the MF thickness and carbonization temperature to obtain an optimal functional skeleton. As shown in Figures S2 and S3, MF sheets with different thickness were achieved by the air suction cutting technique. When the thickness of MF was fixed at 0.1 cm, it showed poor structural stability after carbonization, and carbon fibers were prone to breakage, making it difficult to form a complete sheet. In contrast, an excessively thick MF sheet (e.g., >0.5 cm) tended to accumulate impurity phases at the network junction during the subsequent carbonization process, which reduced the total energy density of composite Li metal anode and was also not conducive to the stable Li

https://doi.org/10.1021/acs.nanolett.5c05102
Nano Lett. 2026, 26, 3330−3337

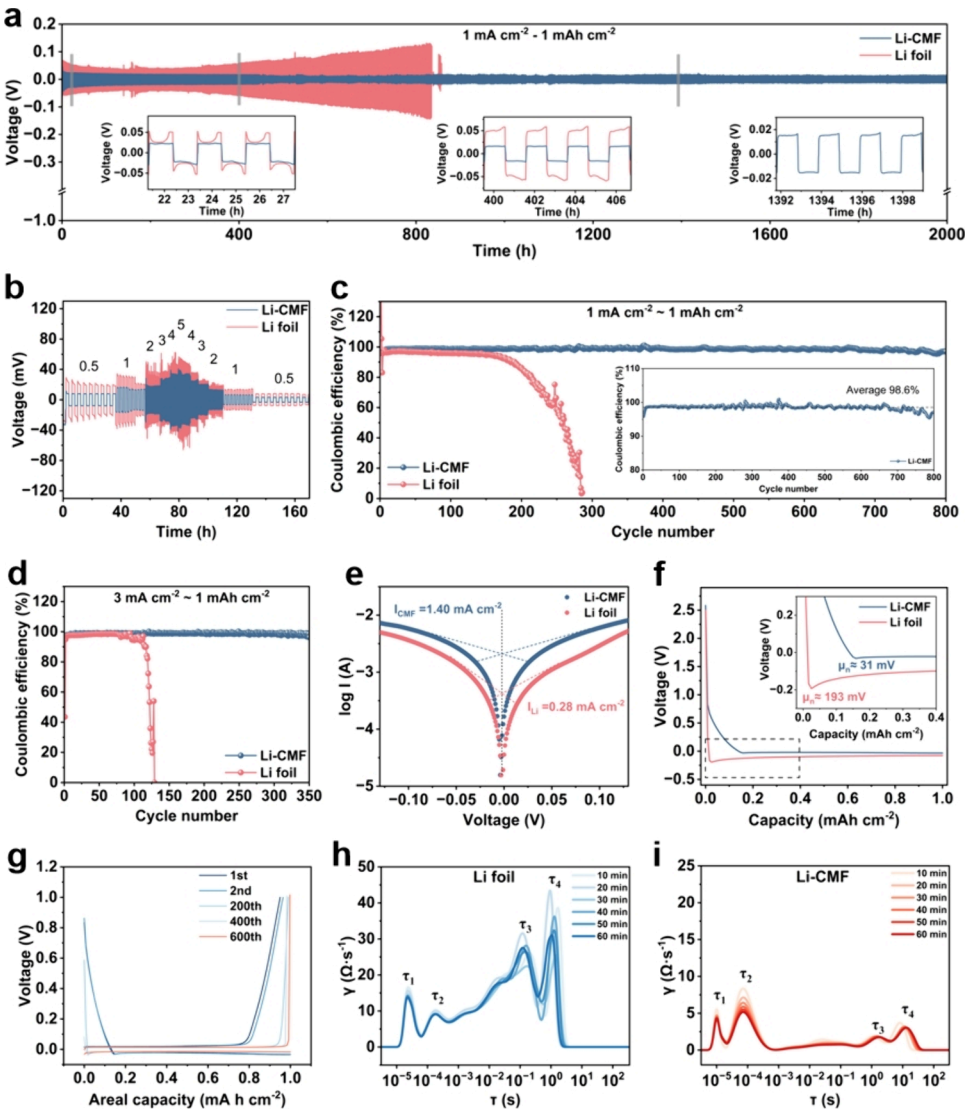

Figure 4. (a) Galvanostatic cycling voltage profiles of CMF and Li anode in symmetric cells at 1 mA cm^{-2} and 1 mAh cm^{-2}. (b) Rate performance at different current densities at a fixed capacity of 1 mAh cm^{-2}. CE comparison of different hosts at (c) 1 mA cm^{-2} and 1 mAh cm^{-2} and (d) 3 mA cm^{-2} and 1 mAh cm^{-2}. (e) Tafel plots of Li||Li cells using Li foil and Li-CMF anodes. (f) Initial voltage−capacity curve of Li||Cu battery at a current density of 1 mA cm^{-2}. (g) Voltage−capacity curves at different cycle numbers. DRT analyses of (h) Li||Li and (i) Li-CMF||Li by in situ EIS.

plating/stripping cycling. Similarly, we also optimized the carbonization temperature of MF. As shown in Figures S4 and S5, combining with thermogravimetric analysis, we found that when the carbonization temperature was 900 °C, the CMF skeleton showed high degree of graphitization and superior cycling stability. Thus, the 0.2 cm thick MF sheet and 900 °C carbonization temperature was used for the subsequent preparation of the CMF skeleton.

Then, EDS and TEM were used to analyze the structural properties of the CMF skeleton. As shown in Figure 2c and Figure S6, C, O, and N elements were uniformly distributed on the surface of CMF fibers. At the same time, HRTEM images displayed that the CMF skeleton had an amorphous carbon structure at the network junctions, while the main body of the fibers possessed ordered domains (Figure 2d and e). This structural feature was consistent with expectations and primarily arose from the difference in carbonization rate and direction between the nodal and fibrous regions during the baking process of organic melamine foam, ultimately leading to local structural heterogeneity and formation of a neuron-like structure. As illustrated in Figures 2f and 2g, this ordered structure effectively alleviated the uneven Li^+-flux distribution in traditional 3D skeleton, and provided continuous and low-hysteresis Li^+ transport pathways, making preferential Li^+ deposition on the fibrous framework. Furthermore, the Li deposition behavior also confirmed that Li preferentially nucleated and deposited on the ordered regions (Figure S7). As shown in Figure S8, the behavior of lithium deposition on CMF observed by in situ optical microscopy also clearly shows that lithium nucleation and growth preferentially occur in fibrous regions containing locally ordered carbon domains.

The selected area electron diffraction (SAED) displayed two diffuse diffraction rings corresponding to the C (002) and C (100) planes (Figure S9), indicating amorphous carbon characteristics, which was consistent with the XRD results (Figure S10). Additionally, in Raman spectra, the peaks located at ∼1350 and 1580 cm^{-1} corresponded to the D-band (associated with structural defects and disordered carbon) and the G-band (attributed to the in-plane vibration of sp^2-hybridized graphitic carbon), respectively. The intensity ratio

https://doi.org/10.1021/acs.nanolett.5c05102
Nano Lett. 2026, 26, 3330−3337

of the D-band to the G-band (I_D/I_G) was 0.99, suggesting the coexistence of both disordered carbon and graphitized carbon, thereby verifying the hybrid microstructure of amorphous and locally ordered carbon regions (Figure 3a).

To investigate the nucleation and deposition behavior, we initially analyzed the existence form of C and lithiophilic N element by XPS. As shown in Figures 3b and 3c, the peak of C 1s spectrum exhibits characteristic peaks at 288.7 eV (C = N), indicating the successful incorporation of nitrogen into the carbon framework. At the same time, the peaks of N 1s at 400.3 and 398.2 eV can be attributed to the pyrrolic N and pyridinic N, respectively, which can provide lithiophilic active sites and effectively regulate Li nucleation behavior, thereby alleviating the interfacial kinetic limitations. Furthermore, the Brunauer−Emmett−Teller (BET) analysis showed that the neuron-like CMF skeleton possessed a high specific surface area of 6.27 $m^2 g^{-1}$ and micropores around 10 nm, which were beneficial for facilitating Li^+ transport within the electrode structure and high Li metal loading (Figure S11). Thus, the composite Li-CMF anode with an areal capacity of 10 mAh cm^{-2} exhibited a thickness of only 82 μm (Figure S12).

Subsequently, the composite Li-CMF anode was submitted to a typical ether-based electrolyte for the Li plating/stripping process at a current density of 1 mA cm^{-2}. As shown in Figure 3d, during the Li plating/stripping process, the corresponding discharging and charging curves exhibited highly stable and flat voltage plateaus as well as low voltage hysteresis, indicating stable interfacial kinetics. Furthermore, the contact angle test also showed that the composite Li-CMF anode had higher electrolyte-philicity (Figure S13). At the same time, the deposition morphology at different cycling stages showed that Li metal was uniformly deposited in the CMF porous framework at the initial stage without Li dendrites. At higher deposition capacities, the interfiber pores were gradually filled, which remained confined within the fiber network. During the Li stripping process, the CMF maintained its stable skeleton (Figure 3e). In contrast, conventional Li foils exhibited numerous cracks and dendritic structures on their surfaces after a similar plating/stripping process (Figure S14). Besides, in situ optical visualization microscopy was also used to further observe the Li plating process. As shown in Figure 3f, at a current density of 5.0 mA cm^{-2}, when using the composite Li-CMF anode, the Li deposition was more uniform, which can be attributed to the featured neuron-like skeleton and abundant lithiophilic sites. In sharp contrast, for bare Li metal anode, an uneven deposition surface with irregular protrusions was formed after only plating for 15 min.

To investigate the electrochemical stability of the composite Li-CMF anode, symmetric cells were employed to evaluate the cycling stability. As shown in Figure 4a, at a current density of 1.0 mA cm^{-2}, the symmetrical Li||Li cells exhibited a continuous voltage fluctuation and failed after only 800 h, indicating unstable Li plating/stripping behavior and the accumulation of dead Li. In contrast, when using the composite Li-CMF anode, the symmetrical cells can maintain a highly stable overpotential for up to 2000 h, demonstrating excellent interfacial stability and enhanced Li plating/stripping reversibility. When the current density was increased to 5.0 mA cm^{-2}, the composite Li-CMF anode can also run stably over 400 h, which was one of the most stable symmetric cells to date (Figure S15). Besides, the rate performance of symmetric cells was also tested under various current densities. As shown in Figure 4b, the composite Li-CMF anode exhibited significantly improved rate performance compared to the bare Li metal anode, featuring lower overpotentials and more stable voltage profiles under various current densities.

The Li|Cu half cells were also assembled to investigate the reversibility of the composite Li-CMF anode. As shown in Figure 4c, at a current density of 1.0 mA cm^{-2}, the composite Li-CMF anode maintained a high average CE of 98.6% throughout 800 cycles, whereas the CE of bare Li metal anode showed drastic fluctuation and even suddenly dropped to <50% after only 150 cycles due to severe interfacial side reactions and dendritic growth. When the current density was increased to 3.0 mA cm^{-2}, the composite Li-CMF anode can also run stably over 350 cycles, whereas the bare Li|Cu half cells experienced rapid CE decay after 80 cycles (Figure 4d).

Then, the interface electrochemical behavior of the composite Li-CMF anode was analyzed by Tafel polarization and electrochemical impedance for investigating its interface ion transport kinetics. As shown in Figure 4e, Tafel polarization curves displayed that the exchange current density of the composite Li-CMF anode (1.4 mA cm^{-2}) was significantly higher than that of the bare Li anode (0.28 mA cm^{-2}), indicating improved charge-transfer kinetics at the electrode/electrolyte interface. Meanwhile, compared to bare Li metal anode, the composite Li-CMF anode demonstrated a much lower overpotential in the initial voltage−capacity curves of Li|Cu cells), highlighting its advantages in reducing charge-transfer resistance and mitigating polarization (Figure 4f). Moreover, the polarization voltage remains basically unchanged with increasing number of cycles, corresponding to high interface stability (Figure 4g). Electrochemical impedance spectroscopy (EIS) showed that the symmetrical cells using the composite Li-CMF anode exhibited lower interfacial resistance both after the first and 50th cycles compared to the symmetrical cells using bare Li metal anode (Figure S16). Moreover, when using the composite Li-CMF anode, the impedance remained relatively low and stable after 50 cycles, while the Li||Li cell displayed a pronounced increase in interfacial resistance, signifying severe interfacial deterioration and poor cycling stability. Furthermore, we also conducted a fitting relaxation time analysis on the EIS results, that was: distribution of relaxation times (DRT). As shown in Figures 4h and 4i, the DRT curves reflect the characteristic time scale of each electrochemical process. The x-axis represents the time constant (τ), which corresponds to the product of resistance (R) and capacitance (C), reflecting the characteristic time scale of each electrochemical process. A smaller τ value indicates a faster reaction rate. The area under each peak is related to the impedance contribution of the corresponding process. As shown in Figure S17, the τ_2 peak of the composite Li-CMF anode was significantly smaller than that of the bare Li anode, suggesting that the composite Li-CMF anode facilitated the formation of a more stable SEI layer. These results collectively suggested that the lithiophilic, neuron-like 3D carbon framework endowed continuous and low-hysteresis Li^+ transport pathways, enhancing interface stability and promoting uniform Li deposition.

Furthermore, XPS was also carried out to analyze the interface stability and SEI film stability. As shown in Figure S18, as the number of cycles increased, the composite Li-CMF anode exhibited a more stable, inorganic-rich SEI layer with a notably higher LiF content. In addition, the SEM image of the cross-section after cycling can also confirm the interface and framework stability. As shown in Figure 5a, after 50 cycles, the

https://doi.org/10.1021/acs.nanolett.5c05102
Nano Lett. 2026, 26, 3330−3337

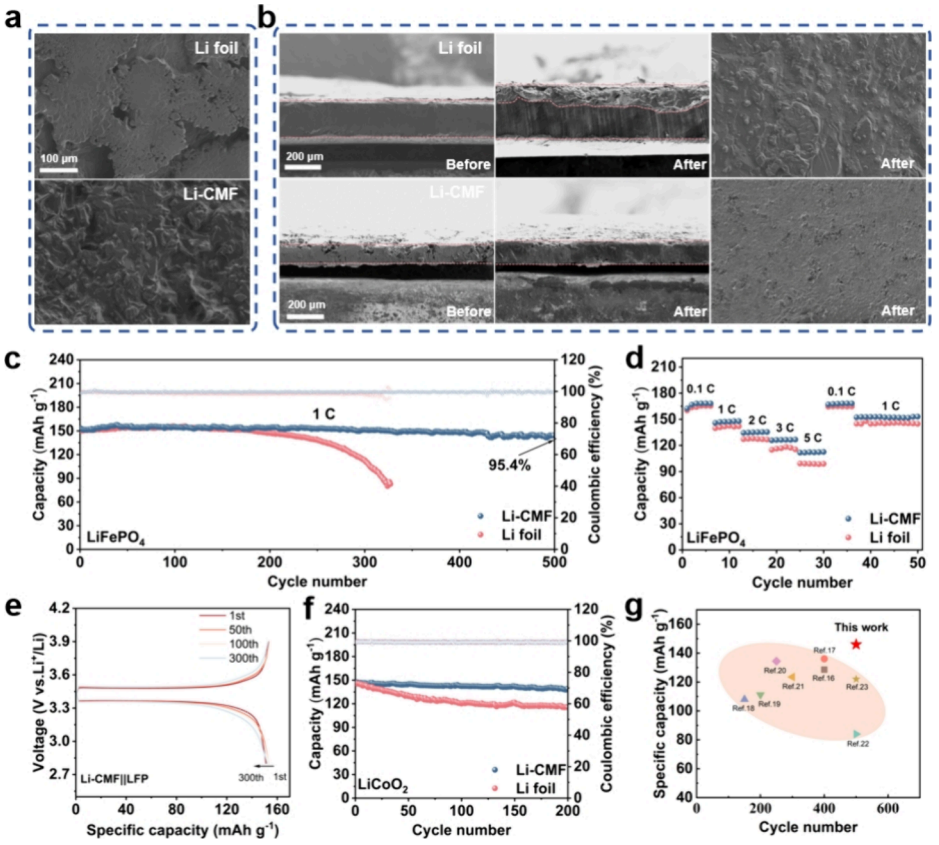

Figure 5. Electrochemical performance and application. (a) Cross-sectional and surface SEM images of Li foil and Li-CMF before and after 50 cycles at current densities of 1 mA cm^{-2} and 1 mAh cm^{-2}. (b) SEM images of Li-CMF and Li foil after depositing at 3 mA cm^{-2} and 1 mAh cm^{-2}. (c) Long cycling performance of LFP||Li-CMF and LFP||Li foil cells at 1 C. (d) Charge−discharge profiles of LFP||Li-CMF with different cycle numbers. (e) Rate performance of commercial LFP||Li-CMF and LFP||Li foil batteries at different current densities. (f) Long cycling performance of LCO||Li-CMF and LCO||Li foil at 1 C. (g) Comparison with recent reports.

thickness of the bare Li metal anode increased from 298 to 417 μm, while the composite Li-CMF anode showed a smaller thickness change, indicating that the introduction of the lithiophilic, neuron-like 3D carbon framework effectively slowed down the volume expansion during charging and discharging process, thereby ensuring the interface stability and framework stability. Besides, the surface of the composite Li-CMF anode remained relatively intact after cycling, whereas numerous cracks and dendrites were observed on the surface of the bare Li metal anode. Morphology comparison at 1 and 3 mA cm^{-2} shows uniform (Figure 5b and Figure S19), dendrite-free deposition on Li-CMF, whereas bare Li foil exhibits severe dendritic growth.

Lastly, to investigate the practical application prospect of the composite Li-CMF anode, the full cells with $LiFePO_4$ as the cathode were assembled. As shown in Figure 5c, the full cells using the composite Li-CMF anode delivered a high capacity of ~150 mAh g^{-1} with a capacity retention of 95.4% after 500 cycles at 1.0 C, significantly outperforming the full cells using bare Li anode and the charge−discharge voltage profiles maintained a stable polarization (Figure 5d). In addition, rate performance tests revealed that the full cells based on the CMF-Li anode displayed an outstanding capacity retention across various current rates from 0.1 to 5.0 C, with excellent recovery when reverting to 1.0 C (Figure 5e). Furthermore, even when paired with the $LiCoO_2$ cathode, the full cells can also achieve stable cycling (Figure 5f). A performance comparison with recently reported on composite Li metal anode also highlighted its practical application prospect (Figure 5g).[16−23]

In summary, we have successfully developed a lithiophilic, neuron-like 3D carbon framework for a Li metal anode, which was achieved by roasting the common N-rich melamine polymer. The abundant N dopants and interconnected conductive architecture synergistically improve the interfacial compatibility between the Li metal and the carbon host, facilitating uniform Li nucleation and suppressing dendritic growth. More importantly, the neuron-like scaffold significantly enhances both electron and ion transport while mitigating interfacial kinetic limitations. As a result, the composite Li metal anode delivered a high CE of 97% over 800 cycles at 1 mA cm^{-2} and 1 mAh cm^{-2} in half cells and maintained a high capacity retention of 95.4% after 500 cycles in full cells. This work provides a promising and practical strategy for improving Li^+ transport kinetics in a composite Li metal anode. Meanwhile, the neuron-like structural design concept can be extended to other metal-based batteries and energy storage systems.

■ ASSOCIATED CONTENT

Data Availability Statement

Data will be made available on request.

Supporting Information

The Supporting Information is available free of charge at https://pubs.acs.org/doi/10.1021/acs.nanolett.5c05102.

https://doi.org/10.1021/acs.nanolett.5c05102
Nano Lett. 2026, 26, 3330−3337

Experimental details, SEM images at different temperatures and thicknesses, in situ optical microscopy observation of Li deposition on CMF, contact angle measurements with electrolyte, EIS, XPS, and SEM images after cycling (PDF)

AUTHOR INFORMATION

Corresponding Authors

Shi Wang − *State Key Laboratory of Flexible Electronics (LoFE), Institute of Advanced Materials (IAM), Nanjing University of Posts and Telecommunications, Nanjing 210023, China; Key Laboratory of Functional Molecular Solids, Ministry of Education, Anhui Engineering Research Center of Carbon Neutrality, College of Chemistry and Materials Science, Anhui Normal University, Wuhu 241000, china;* orcid.org/0000-0002-5331-413X; Email: iamshiwang@njupt.edu.cn

Yinghui Wei − *College of Materials Science and Engineering, Taiyuan University of Technology, Taiyuan 030024 Shanxi, China*; Email: weiyinghui@tyut.edu.cn

Qian Wang − *College of Materials Science and Engineering, Taiyuan University of Technology, Taiyuan 030024 Shanxi, China;* orcid.org/0000-0001-5161-6241; Email: qianwang0825@pku.edu.cn

Zhong Jin − *MOE Key Laboratory of High Performance Polymer Materials and Technology, Jiangsu Key Laboratory of Green Energy Catalysis and Intelligent Chemical Engineering, Suzhou Key Laboratory of Green Intelligent Manufacturing of New Energy Materials and Devices, Tianchang New Materials and Energy Technologies Research Center, Institute of Green Chemistry and Engineering, School of Chemistry and Chemical Engineering, Nanjing University, Jiangsu 210023, China;* orcid.org/0000-0001-8860-8579; Email: zhongjin@nju.edu.cn

Authors

Bo Zhang − *College of Materials Science and Engineering, Taiyuan University of Technology, Taiyuan 030024 Shanxi, China*

Donghu Li − *College of Materials Science and Engineering, Taiyuan University of Technology, Taiyuan 030024 Shanxi, China*

Xinli Wu − *Hubei Key Laboratory of Green Intelligent Manufacturing Technologies of Battery Key Materials, Shiyan 442500, China*

Jitao Huang − *College of Chemistry and Materials, Ningde Normal University, Ningde, Fujian 352100, China*

Lifeng Hou − *College of Materials Science and Engineering, Taiyuan University of Technology, Taiyuan 030024 Shanxi, China*

Complete contact information is available at: https://pubs.acs.org/10.1021/acs.nanolett.5c05102

Author Contributions

[▽]Bo Zhanga and Donghu Lia contributed equally to this work.

Notes

The authors declare no competing financial interest.

ACKNOWLEDGMENTS

This work was supported by the National Natural Science Foundation of China (22402146, 22572140, U25A20628, 22561160129, 22479074, and 22475096), the Beijing Natural Science Foundation Xiaomi innovation joint Foundation (L223011), the Young Elite Scientists Sponsorship Program by CAST(2022QNRC001), the Fundamental Research Program of Shanxi Province (202103021222006), the Shanxi Energy Internet Research Institute (SXEI2023A004), the Open Research Fund of Guangdong Advanced Carbon Materials Co., Ltd. (Kargen-2024B0905), the Open Fund of Key Laboratory of Functional Molecular Solids of Ministry of Education (FMS2025009), the Equipment Pre-Research and Ministry of Education Joint Fund (8091B02052407), the Fundamental Research Program Key Project of Jiangsu Province (BK20253008), the Natural Science Foundation of Jiangsu Province (BK20240400, BK20241236), the Science and Technology Major Project of Jiangsu Province (BG2024013), the Scientific and Technological Achievements Transformation Special Fund of Jiangsu Province (BA2023037), the Academic Degree and Postgraduate Education Reforming Project of Jiangsu Province (JGKT24_C001), the Key Core Technology Open Competition Project of Suzhou City (SYG2024122), the Open Research Fund of Suzhou Laboratory (SZLAB-1308-2024-TS005), the Chenzhou National Sustainable Development Agenda Innovation Demonstration Zone Provincial Special Project (2023sfq11), and the Natural Science Foundation of NJUPT (NY223079, NY224119).

REFERENCES

(1) Yan, X.; Lin, L.; Chen, Q.; Xie, Q.; Qu, B.; Wang, L.; Peng, D. L. Multifunctional roles of carbon-based hosts for Li-metal anodes: A review. *Carbon Energy* **2021**, *3* (2), 303−329.

(2) Albertus, P.; Babinec, S.; Litzelman, S.; Newman, A. Status and challenges in enabling the lithium metal electrode for high-energy and low-cost rechargeable batteries. *Nature Energy* **2018**, *3* (1), 16−21.

(3) Wang, Q.; Lu, T.; Liu, Y.; Dai, J.; Guan, L.; Hou, L.; Du, H.; Wei, H.; Liu, X.; Han, X.; Ye, Z.; Zhang, D.; Wei, Y.; Zhou, H. Li+ migration and transformation at the interface: A review for stable Li metal anode. *Energy Storage Materials* **2023**, *55*, 782−807.

(4) Wang, Z.; Wang, H.; Qi, S.; Wu, D.; Huang, J.; Li, X.; Wang, C.; Ma, J. Structural regulation chemistry of lithium ion solvation for lithium batteries. *EcoMat* **2022**, *4* (4), No. e12200.

(5) Wei, T.; Lu, J.; Zhang, P.; Zhang, Q.; Yang, G.; Yang, R.; Chen, D.; Wang, Q.; Tang, Y. An intermittent lithium deposition model based on bimetallic MOFs derivatives for dendrite-free lithium anode with ultrahigh areal capacity. *Chin. Chem. Lett.* **2024**, *35* (8), 109122.

(6) Zhang, A.; Fang, X.; Shen, C.; Liu, Y.; Zhou, C. A carbon nanofiber network for stable lithium metal anodes with high Coulombic efficiency and long cycle life. *Nano Research* **2016**, *9* (11), 3428−3436.

(7) Zhang, R.; Cheng, X. B.; Zhao, C. Z.; Peng, H. J.; Shi, J. L.; Huang, J. Q.; Wang, J.; Wei, F.; Zhang, Q. Conductive Nanostructured Scaffolds Render Low Local Current Density to Inhibit Lithium Dendrite Growth. *Adv. Mater.* **2016**, *28* (11), 2155−2162.

(8) Hui, Y.; Wu, Y.; Sun, W.; Sun, X.; Huang, G.; Na, Z. Nanosecond Pulsed Laser-Assisted Deposition to Construct a 3D Quasi-Gradient Lithiophilic Skeleton for Stable Lithium Metal Anodes. *Adv. Funct. Mater.* **2023**, *33* (34), 2303319.

(9) Sun, Z.; Jin, S.; Jin, H.; Du, Z.; Zhu, Y.; Cao, A.; Ji, H.; Wan, L. J. Robust Expandable Carbon Nanotube Scaffold for Ultrahigh-Capacity Lithium-Metal Anodes. *Adv. Mater.* **2018**, *30* (32), 1800884.

(10) Yu, J.; Wang, Y.; Kong, L.; Chen, S.; Zhang, S. Neuron-Mimic Smart Electrode: A Two-Dimensional Multiscale Synergistic Strategy for Densely Packed and High-Rate Lithium Storage. *ACS Nano* **2019**, *13* (8), 9148−9160.

(11) Liu, T.; Hu, Q.; Li, X.; Tan, L.; Yan, G.; Wang, Z.; Guo, H.; Liu, Y.; Wu, Y.; Wang, J. Lithiophilic Ag/Li composite anodes via a

spontaneous reaction for Li nucleation with a reduced barrier. *Journal of Materials Chemistry A* **2019**, *7* (36), 20911−20918.
(12) Chi, S.-S.; Wang, Q.; Han, B.; Luo, C.; Jiang, Y.; Wang, J.; Wang, C.; Yu, Y.; Deng, Y. Lithiophilic Zn Sites in Porous CuZn Alloy Induced Uniform Li Nucleation and Dendrite-free Li Metal Deposition. *Nano Lett.* **2020**, *20* (4), 2724−2732.
(13) Liu, H.; Chen, X.; Cheng, X. B.; Li, B. Q.; Zhang, R.; Wang, B.; Chen, X.; Zhang, Q. Uniform Lithium Nucleation Guided by Atomically Dispersed Lithiophilic CoN_x Sites for Safe Lithium Metal Batteries. *Small Methods* **2019**, *3* (9), 1800354.
(14) Wang, S. H.; Yin, Y. X.; Zuo, T. T.; Dong, W.; Li, J. Y.; Shi, J. L.; Zhang, C. H.; Li, N. W.; Li, C. J.; Guo, Y. G. Stable Li Metal Anodes via Regulating Lithium Plating/Stripping in Vertically Aligned Microchannels. *Adv. Mater.* **2017**, *29* (40), 1703729.
(15) Song, L.; Zhang, H.; Yang, N.; Wu, N.; Yao, H.; Zhang, R.; Zhang, G. Radially unfolded nanosheets in polyacrylonitrile nanofibers: A biomimetics construct of high-performance anode for lithium-ion batteries. *Carbon* **2025**, *237*, 120145.
(16) Chen, D.; Chen, C.; Yu, H.; Zheng, S.; Jin, T.; Li, N. W.; Yu, L. Formation of N-Doped Carbon Nanofibers Decorated with MoP Nanoflakes for Dendrite-Free Lithium Metal Anode. *Adv. Funct. Mater.* **2024**, *34* (38), 2402951.
(17) Zhuang, H.; Zhang, T.; Xiao, H.; Liang, X.; Zhang, F.; Deng, J.; Gao, Q. 3D Free-Standing Carbon Nanofibers Modified by Lithiophilic Metals Enabling Dendrite-Free Anodes for Li Metal Batteries. *Energy & Environmental Materials* **2023**, *6* (3), No. e12470.
(18) Chen, C.; Guan, J.; Li, N. W.; Lu, Y.; Luan, D.; Zhang, C. H.; Cheng, G.; Yu, L.; Lou, X. W. Lotus-Root-Like Carbon Fibers Embedded with Ni−Co Nanoparticles for Dendrite-Free Lithium Metal Anodes. *Adv. Mater.* **2021**, *33* (24), 2100608.
(19) Peng, G.; Zheng, Q.; Luo, G.; Zheng, D.; Feng, S. P.; Khan, U.; Akbar, A. R.; Luo, H.; Liu, F. A Gradient Lithiophilic Structure for Stable Lithium Metal Anodes with Ultrahigh Rate and Ultradeep Capacity. *Small* **2023**, *19* (47), 2303787.
(20) Fang, Y.; Zhang, S. L.; Wu, Z.-P.; Luan, D.; Lou, X. W. A highly stable lithium metal anode enabled by Ag nanoparticle−embedded nitrogen-doped carbon macroporous fibers. *Science Advances* **2021**, *7* (21), No. eabg3626.
(21) Wang, J.; Yao, S.; Tao, R.; Liu, X.; Geng, J.; Hong, C.; Li, H.; Yu, G.; Li, H.; Sun, X.-G.; Li, J.; Liang, J. Lithiophilic CoF_2@C hollow spheres towards spatial lithium deposition for stable lithium metal batteries. *Journal of Energy Chemistry* **2024**, *97*, 55−67.
(22) Zhang, X.; Zhou, L.; Hu, K.; Gao, D.; Tang, S.; He, L.; Chen, Y.; Zhang, P.; Zhang, Z. Uniform lithium deposition regulated by lithiophilic Mo_3N_2/MoN heterojunction nanobelts interlayer for stable lithium metal batteries. *Chemical Engineering Journal* **2023**, *476*, 146612.
(23) Shen, X.; Shi, S.; Li, B.; Li, S.; Zhang, H.; Chen, S.; Deng, H.; Zhang, Q.; Zhu, J.; Duan, X. Lithiophilic Interphase Porous Buffer Layer toward Uniform Nucleation in Lithium Metal Anodes. *Adv. Funct. Mater.* **2022**, *32* (39), 2206388.

https://doi.org/10.1021/acs.nanolett.5c05102
Nano Lett. 2026, 26, 3330−3337